2

Electron Emission from Surfaces Induced by Slow Ions and Atoms

R.A. Baragiola and P. Riccardi

2.1 Introduction

Electron emission from surfaces is of crucial importance in determining the properties of electrical discharges, where it is caused by the impact of ions, atoms, electrons, and photons. At the microscopic level, the physics of electron emission from solid targets is usually described by a three-step model: electron excitation, electron transport to the surface, and its escape through the surface. This division serves a heuristic purpose and it must be borne in mind that, in purely surface events, actually only one step is involved. What distinguishes electron emission by different incoming particles is the excitation step [1], which depends strongly on the momentum of the particle. This is because there is a minimum energy needed to extract an electron from the solid (work function for metals, band gap plus electron affinity for nonmetals) and this energy transfer implies a momentum transfer from the projectile.

This chapter is concerned with heavy particle collisions (ions and atoms) at low energies (below a few keV) and will discuss first the physical mechanisms and then applications to electrical discharges in gases. The overall picture of electron emission induced by heavy particles is the following. Electrons are excited from the target or the projectile as a result of Coulomb interactions involving the nuclei and electrons through mechanisms that are grouped in two categories, potential and kinetic, depending on the source of the excitation energy. Such excitations occur mostly in binary collisions at the surface or very shallow depths, since the penetration depth of low-energy atomic projectiles is usually very shallow, tens of nm or less. The excited electrons can be ejected directly into vacuum or undergo a series of collisions in the target solid (electron transport) on their way to the surface. The collisions are either elastic scattering with atomic cores, which cause large deflections in trajectories, or energy loss collisions by scattering with other electrons, contingent on the availability of electronic states. As a result of such inelastic scattering, the electrons which succeed in escaping the solid come from a shallow depth, of the order of 2 nm for metals and semiconductors and up to a few tens of

nm for insulators. In the latter case, the depth of origin of electrons is limited, at low primary energies, by the slowing down of the projectile mainly as a result of ion–atom collisions. Electron escape involves energy loss through the surface barrier and change of momentum perpendicular to the surface.

The main observable in electron emission is the average electron yield γ (number of electrons ejected per primary particle), either as an integral quantity or in the form of distributions of electrons according to their energies, angles of emission, and spin state. Emission events are statistically distributed; i.e., the yield fluctuates around the mean value γ and is described by probabilities P_n of emission of n electrons per projectile ($\sum P_n = 1$; $\sum nP_n = \gamma$). At the low impact velocities of interest, only low n (0, 1, 2) are important [2]. Experiments show that γ is at most $\sim$2–3 and depends critically on the electronic structure of the surface. Large increases in γ are detected when going from clean metals to gas-covered surfaces. The energy of emitted electrons is less than 20 eV, typically peaking at a few eV, while the distribution of emission angles with respect to the surface normal is cosine or below cosine. For single crystals, the angular distribution is strongly affected by diffraction.

2.2 Physical Mechanisms

The fundamental physics of electron emission in slow ion–surface interactions has been reviewed in detail, with emphasis on atomically clean surfaces. See reviews in books [3–7] and specific articles on kinetic [8,9] and potential [10,11] electron emission. Here, the focus will be on slow singly charged ions mostly impacting gas-covered surfaces, typical of electrical discharges.

2.2.1 Excitation Mechanisms

In the impact energy range of interest, two main electron excitation mechanisms can be broadly distinguished, kinetic and potential, depending on whether the excitation energy is provided by the motion of the projectile or its potential energy. The potential and kinetic emission mechanisms are not exclusive of collisions at surfaces but also happen in two-body gas-phase collisions. Both mechanisms can only occur above an energy threshold related to U, the minimum energy required to free an electron. It is typically assumed that the electron comes from the surface and has a binding energy that is not much affected by the incoming particle. This is a good approximation for metals, where U is equal to the work function and falls in the approximate range 1.5–6 eV. In nonmetals (semiconductors and dielectrics), U is often approximated by the minimum binding energy of a valence electron, as usually it costs less energy to remove an electron from the solid than from the incoming atomic particle (its ionization potential). In this case, U is equal to the surface band gap plus the electron affinity. Values range approximately from 4 to 11 eV.

In potential electron emission (PEE), electron excitation results from the conversion of internal energy ε brought by an ion or an excited atom, through a two-electron Auger process. Such process can be Auger capture where an electron from the solid is captured by the ion and another electron is excited or Auger deexcitation where an excited projectile relaxes to a lower state transferring the energy to another electron. For electron emission to occur, the energy released in the Auger process, $\varepsilon - U$, has to exceed U (i.e., emission requires $\varepsilon > 2U$). For most singly charged ions, PEE does not occur at surfaces that have been exposed to the atmosphere, since the relation $\varepsilon > 2U$ is not generally satisfied for adsorbed molecules.

In kinetic electron emission (KEE), electrons are excited as a consequence of time-varying Coulomb interactions between the nuclei and electrons of the incident particle and the surface, within the constraints of the Pauli exclusion. Here, several mechanisms are possible, depending on the type of surface. In metals, projectiles can interact with loosely bound ("conduction") electrons and shallow core levels (such as the d-band in light transition metals). Deeper core levels are not accessible at the energies of interest. Binary collisions of "free" valence electrons of the targets with the screened Coulomb field of the projectile are the dominant excitation mechanism for light projectiles (H, He, Li) on metals. A collision with a nearly free electron cannot result in a large energy transfer because the mass mismatch between the heavy particle and the electron prevents transferring sufficient momentum. The maximum energy transfer to an electron by a much heavier atomic particle occurs in head on collisions, where the electron gains twice the projectile velocity after a single scattering. The resulting energy transfer is $T = 2mv(v + v_\mathrm{e})$, where v and v_e are the velocity of the projectile and the target electron before the collision, respectively, and m the electron mass. Therefore, there is a minimum impact velocity that will result in a free electron excited to a state with energy above the vacuum level, when $T = W$, given by [12]

$$v_\mathrm{th} = \frac{v_\mathrm{F}}{2}\left(\sqrt{1 + \frac{2W}{mv_\mathrm{F}^2}} - 1\right), \tag{2.1}$$

where W is the work function, v_F the Fermi velocity, and m the electron mass. This corresponds to $1.5\text{–}3 \times 10^7\,\mathrm{cm\ s^{-1}}$ (117–470 eV amu^{-1}) for most metals, consistent with extrapolation of the experimental results for light projectiles [12]. Deviations from (2.1) contain information on the velocity distribution of electrons at the surface [13].

For heavy projectiles, the observed threshold velocities are an order of magnitude lower than (2.1). This is due to an additional electron excitation mechanism. This is the electron–electron interactions during the interpenetration of the electron clouds of the projectile and one of the target atoms which promote electronic levels directly into the ionization continuum or through autoionizing states [14].

A direct demonstration of the importance of excitations in such binary atom–atom collisions below the free electron threshold of (2.1) was made by Rabalais et al. [15] who studied the impact parameter dependence of KEE in collisions of 4 keV Ar^+ with Ni(110) and found that electron emission required a minimum impact parameter in a collision below 0.3 Å.

In binary collisions between projectile and a target atom, the minimum possible threshold for KEE allowed by energy conservation is when the center-of-mass energy equals U. However, quite above this threshold the electron yield is usually undetectable above the background of other secondary processes.

2.2.2 Separation of PEE and KEE

PEE and KEE are separable in two limiting cases. When $E_{\rm cm} < U$, and $\varepsilon > 2U$, only PEE can occur. If, on the other hand, $\varepsilon < 2U$ and $E_{\rm cm} > U$, electrons can only be ejected by the kinetic mechanism. In KEE, the threshold condition is when the maximum energy transfer is equal to U. Energy transfer center-of-mass energy $E_{\rm cm}$ has to exceed U. PEE does not require the motion of the projectile but can be affected by it, whereas KEE can be affected by the degree of excitation of the projectile. Electron emission statistics have been used to separate PEE and KEE for singly charged ions, based on the fact that PEE generally results in at most one electron being emitted [16].

2.2.3 Electron Transport and Escape into Vacuum

At low projectile impact energies, many of the electrons are emitted from the surface layer and it is difficult or incorrect to separate scattering inside the solid and transmission through the surface barrier. Inside the solid, excited electrons undergo a cascade of collisions until their energy is degraded into heat or stored in long-lived excited states. Those excited electrons which are directed outward may cross the surface of the solid and escape before being thermalized, giving rise to electron emission. Therefore, the energy distribution of emitted electrons does not represent an equilibrium situation. An important characteristic of the low-energy ion impact case discussed here is that the vast majority of the initially excited electrons have very small kinetic energies, insufficient to excite additional electrons above the vacuum level. That is, electron multiplication [17] is typically unimportant.

2.3 Electron Yields

Experiments involve measuring the dependence of electron emission on different factors. These include the projectile and target properties and the bombardment geometry. Important properties of the projectile are its excitation and ionization state, its mass, and whether it comes as a single atom,

a molecule, or a cluster of atoms. Relevant target properties are the elemental composition and atomic and electronic structure in the surface region, the magnitude of surface electric fields, the temperature, and, for magnetic materials, the degree of magnetization. The relevant geometrical factors in experiments include the angle of incidence with respect to the surface and to the possible preferred crystallographic planes.

Electrons can absorb a much larger energy transfer (even a substantial fraction of the center-of-mass energy in the collision) if they are not free, but bound to atoms. In this case, the treatment of the collision is similar to that of ionization in gas-phase collisions, where electronic excitations occur due to electron–electron interactions which promote electronic levels directly into the ionization continuum or through autoionizing states [5]. Atom–atom collisions can excite electrons from the projectile or the target and are thought to be the main mechanism ejecting electrons during impacts on gas-covered surfaces [18]. The atomic collisions considered here can occur between a projectile atom and a target atom, between fast target recoils and other atoms, or even between atoms in the projectile in the collision spike formed on impact.

2.3.1 Dependence of the Electron Yields on Ion Velocity

Early measurements using atomic ions have shown that, at low velocities, the KEE yields have the velocity dependence

$$\gamma = \gamma_{\mathrm{o}}(v - v_{\mathrm{th}}), \tag{2.2}$$

for ν not too close to ν_{th}. The extrapolated value of ν_{th} is $\sim 4.5 \times 10^6\,\mathrm{cm\ s^{-1}}$ ($10.6\,\mathrm{eV\ amu^{-1}}$) for gas-covered surfaces [19, 20], roughly independent of the type of bombarding ions. The implicit acceptance of (2.2) has influenced the way data have been plotted in the literature. One can ask whether the extrapolated value ν_{th} is affected by a limited experimental sensitivity or the way the data are plotted. KEE yields induced by Xe^+ ions on atomically clean gold [21, 22] depart from the linear behavior of (2.2) and do not have a definite threshold down to $\nu = 1.2 \times 10^6\,\mathrm{cm\ s^{-1}}$ (100 eV). KEE down to $1.5 \times 10^6\,\mathrm{cm\ s^{-1}}$ (160 eV) has previously been observed by Waters [23] for Cs on W who also found that gas adsorption increases the electron yields by three orders of magnitude at these low velocities. We will return to this last point later, because of its significance for discharges.

The model of KEE resulting from binary low velocity atomic collisions suggests that the projectile velocity be measured in terms of the characteristic velocity

$$v_{\mathrm{c}} = \frac{a\Delta E}{\hbar}, \tag{2.3}$$

which follows from Massey's [24] adiabatic criterion, where a is the range of the interaction causing the transition with energy defect ΔE. At low velocities,

this suggests a similar dependence that has been proposed for ionization collisions in the gas phase, using a straight-path approximation [25, 26],

$$\gamma = \gamma_o \exp(-v_c/v), \tag{2.4}$$

or a sum of exponentials if several processes are present with different values of ν_c. Breaks in the plot of $\log \gamma$ vs. $1/\nu$ could then be used to identify different excitation channels.

In the limit of very low velocities, (2.4) should break down for at least two reasons (1) the inability to reach interatomic distances where the coupling to the continuum is sufficiently strong and (2) the existence of an absolute binary threshold when the center-of-mass energy equals U. Situations close to this absolute binary threshold have been identified in the impact of relatively light ions on gas-covered surfaces [18], from comparisons with gas-phase ionization cross sections.

Beyond the binary collision approximation, the minimum possible threshold results from energy conservation, when the projectile energy equals U. For this to occur, the lattice has to absorb all the momentum of the projectile and all the available energy has to go into the excitation of a single electron. This is very unlikely for heavy particle impact, since there is a large number of alternative pathways for the dissipation of the incident energy.

2.3.2 Electron Energy and Angular Distributions

Ferrón et al. [27] have measured electron energy distributions for 4 keV Ar^+ on clean and oxidized Al and Mo surfaces. The peak of the distributions occurs at a few eV and there are relatively fewer high-energy electrons from oxidized surfaces. Other collision systems are characterized by electron energy distributions with sharp or broad peaks characteristic of specific processes, such as autoionization, plasmon decay, or the decay of shallow core levels [5]. Recently, the method of factor analysis of energy distribution curves has been used to identify different mechanisms of ion-induced electron emission [28].

The angular distribution of ejected electrons has, in general, a cosine dependence on angle with respect to the surface normal. Structure is superimposed on this dependence in the case of experiments on single crystals, due to the diffraction of the electrons [29].

2.3.3 Electron Emission from Contaminant Surface Layers

Figure 2.1 depicts the results of analytical expressions given by Phelps and Petrovic [30] for electron yields γ_i (γ_a) from metal surfaces under the impact of Ar^+ ions (Ar neutrals) both for clean and contaminated (dirty) surfaces, based on a compilation of experimental data. This graph serves to illustrate several points. For Ar^+ on clean surfaces, the electron yields are constant at very low energies, indicating the predominance of PEE. In contrast, Ar neutrals,

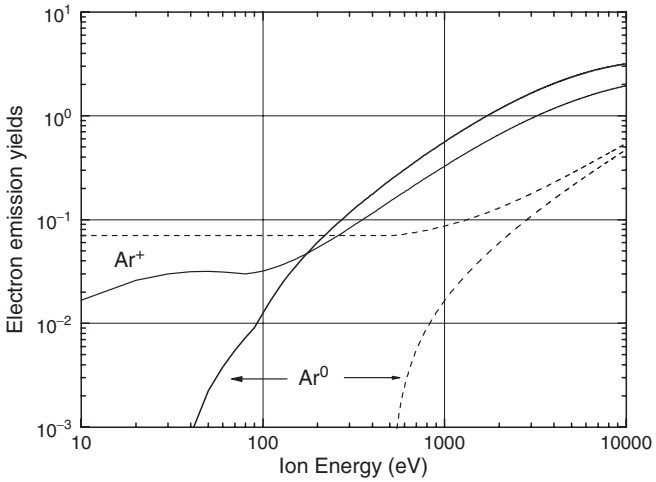

Fig. 2.1. Electron emission yields for argon ion and atom bombardment for clean (*dashed curves*) and dirty (*continuous curves*) metal surfaces (adapted from [30])

which carry no potential energy, do not produce PEE. The electron yields for neutrals are exclusively due to KEE and increase rapidly with energy above a threshold which is below 40 eV. The KEE component of Ar^+ is essentially the same as that of Ar, due to the spatial separation of the PEE and KEE mechanisms. PEE occurs outside the surface by Auger neutralization producing neutral Ar which then enters the solid producing KEE. For dirty surfaces, the PEE yield by Ar^+ is suppressed, a general property of PEE caused by the stronger bonding of electrons in adsorbates compared to metals. Strikingly, the KEE yield, seen clearly for neutral Ar, is much larger for dirty than for clean surfaces and the ratio decreases with increasing projectile energy, as reported earlier [31].

This behavior of dirty surfaces is similar to that of insulators which also have larger KEE yields than for clean metals or semiconductors. In most of the literature, this is attributed to a larger mean electron escape depth due to the reduced electron scattering for electron energies below the band gap. However, this effect is not important at the low energies appropriate to electron discharges, where ion penetration is very shallow. A more important factor is the easier electron escape from insulators due to a reduced surface barrier.

Comparative experiments on the adsorption of oxygen on clean Al and Mo surfaces showed very large effects on the yields [27] with γ increasing for Al and decreasing for Mo. Since one can expect a similar electronic configuration in the oxygen in both cases, the reason for the large differences in the two materials is not likely to result from differences in direct excitation. Rather, it was argued that yields were mainly affected by the change in the surface barrier but not necessarily related to changes in the work function.

2.4 The Role of Ion-Induced Electron Emission in Glow Discharges

The pivotal role of electron emission yields in electrical discharges has become better understood in the last decades. Recent complex numerical models [32–39], categorized as fluid, kinetic (Monte Carlo), and hybrid (combination), have shown that the modeled discharge characteristics are seriously influenced by the accuracy of the input data. Models require realistic cross sections for electron, ion, atom and photon collisions with the gas, as well as realistic probabilities for electron, ion, atom and photon interactions with electrode surfaces. Whereas the data for modeling the relevant gas-phase processes are relatively well known [30, 39, 40], those describing electrode processes are often uncertain, such as the electron emission yields from cathode materials under actual gas discharge conditions. Therefore, there has been significant effort spent lately in understanding issues associated with secondary electron emission processes in modeling the characteristics of gas discharges [30,40–45].

A comparison with measured voltage–current characteristics is generally the first way to check the results of model calculations. An important parameter is the ratio of the electron to ion current densities at the cathode surface, $\gamma' = J_{\mathrm{e,tot}}/J_{\mathrm{i,tot}}$, called the *apparent* or *effective* secondary electron emission yield per ion. The derivation of this quantity is not trivial, since several particles (positive ions, metastable atoms, fast neutrals, and photons) contribute to electron emission from the cathode and their relative importance changes with the operating parameters and conditions of the discharge. Furthermore, as compared with ion beam measurements of electron emission yields of heavily sputtered samples in ultrahigh vacuum, cathode materials operated under discharge conditions can have significantly different secondary emission yields [30]. Nevertheless, until recently, it was common practice to assume a value of γ' independent of discharge conditions. An example of the effect of the choice of γ' is shown in Fig. 2.2, taken from [39], depicting the voltage–current density curve of the helium discharge for $pL = 3$ Torr cm, where p is the pressure and L the electrode separation.

The simulation is based on a 1D hybrid model, using different values of γ'. As can be seen from Fig. 2.2, the particular choice of the value of γ' results in pronounced differences in the calculated curves, none of which are consistent with experimental data. We note that the curve obtained assuming $\gamma = 0.3$, a value that corresponds to typical electron yields for He^+ on clean metal surfaces, disagrees strongly with the experimental data. Figure 2.2 reports also the characteristic obtained from a fluid model calculation, using $\gamma' = 0.16$. It agrees quite well with experiment, suggesting that cathode was not cleaned by the low-sputtering yield of He since contaminated surfaces have low PEE yields. However, as discussed in [39], the fluid model fails to reproduce other characteristics of the discharge, such as the spatial distributions of ion and electron densities.

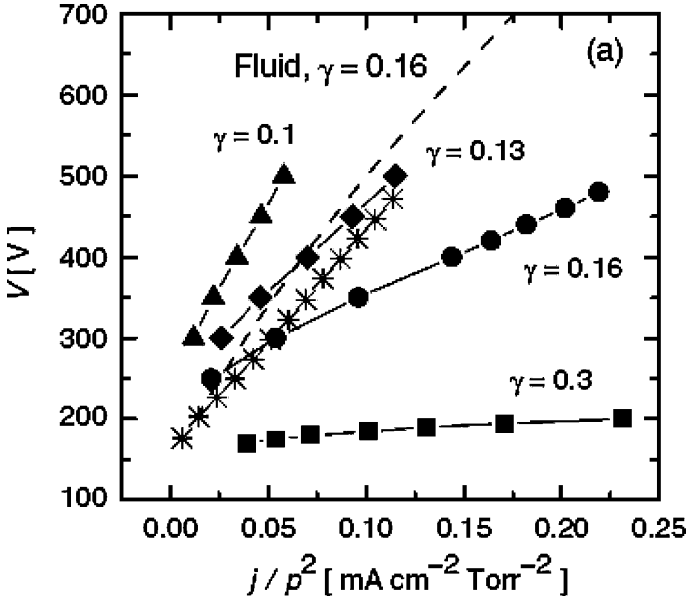

Fig. 2.2. Electrical characteristics of helium glow discharges. The 1D hybrid modeling results (*filled symbols*) obtained for $pL = 3$ Torr cm are shown for apparent secondary electron yield values $\gamma = 0.1$, 0.13, 0.16, and 0.3. kTe = 0.3 eV is assumed in the model. The *dashed line* is the result of a fluid calculation with $\gamma = 0.16$ and kTe = 1 eV, while *asterisk* denotes experimental data obtained at $pL = 3.38$ Torr cm (from [39])

Phelps and Petrovic [30] reviewed the processes responsible for the production of the initial secondary electrons required for the growth of current at electrical breakdown and for the maintenance of cold-cathode discharge in argon, a commonly used as a benchmark gas for discharge studies. These electrons are produced in collisions of Ar ions, fast Ar atoms, metastable atoms, or photons with the cathode or in ionizing collisions of fast atoms or ions with the neutral Ar atoms in the gas phase. Since electron emission yields for ions, fast atoms, metastable atoms, and photons vary greatly with particle energy, surface conditions and discharge conditions, the effective yield γ' has to include the effect of all the relevant mechanisms as accurately as possible. The authors assembled a large amount of data for photoelectric yields and secondary electron emission yields by argon ions and fast argon atoms, as a function of ion and atom energy, for a large number of different metal surfaces, both clean and dirty. Since data for different metal surfaces are rather close to each other, they made analytical fits [30, 46] for electron emission yields as a function of impact energy for both clean and dirty surfaces, as shown in Fig. 2.1. The fits should be best for KEE yields from contaminated surfaces

because of the insensitivity to the target material. For clean surfaces, it is better to use the PEE yield from the fit to a large number of materials [47]

$$\gamma_{\mathrm{p}} = 0.032(0.78E_{\mathrm{i}} - 2\phi). \tag{2.5}$$

Here E_{i} is the neutralization energy of the ion and ϕ the work function of the surface. For contaminated surfaces, the PEE is quite smaller, as shown in Fig. 2.1 for Ar^+ (Ar^0 only produces KEE). In this case, there is no equivalent expression to (2.5) since yields depend not only on ϕ but also on the type of contaminant.

The analytical expressions provided by Phelps and Petrovic stimulated several studies that improved the description of discharge processes in argon [30, 39, 41–45]. Given the energy-dependent electron yields for each relevant process, the apparent yield can be calculated self-consistently from the simulation. As an example of the procedure, we mention here the work by Bogaerts and Gijbels [41] who developed a hybrid model to describe the discharge conditions typically used for analytical glow discharge mass spectrometry. In this technique, the material under analysis is used as the cathode of the glow discharge, and the particles sputtered by energetic plasma species are identified by mass analysis. Under the typical conditions of such a discharge, only Ar^+ and fast Ar play a significant role in electron emission from the cathode. Hence the apparent yield can be calculated from the simulation as

$$\gamma' = \frac{J_{\mathrm{e,tot}}}{J_{\mathrm{i,tot}}} = \frac{\int_0^{E_{\mathrm{i,max}}} F_{\mathrm{i}}(E)\gamma_{\mathrm{i}}(E)\mathrm{d}E + \int_0^{E_{\mathrm{a,max}}} F_{\mathrm{a}}(E)\gamma_{\mathrm{a}}(E)\mathrm{d}E}{\int_0^{E_{\mathrm{i,max}}} F_{\mathrm{i}}(E)\mathrm{d}E}, \tag{2.6}$$

where $\gamma_{\mathrm{i}}(E)$ and $\gamma_{\mathrm{a}}(E)$ are the yields induced by ions and atoms shown in Fig. 2.1 while $F_{\mathrm{i}}(E)$ and $F_{\mathrm{a}}(E)$ are the calculated ion and atom flux energy distribution at the cathode. The energy distributions $F_{\mathrm{i}}(E)$ and $F_{\mathrm{a}}(E)$ depend on discharge conditions and may significantly affect the value of the effective yield. For example, the model of Phelps and Petrovic calculates the effective yield describing the fluxes of electrons, ions, atoms, and photons in a spatially uniform electric field. Attempts have been made to use this effective electron yield, calculated for a uniform electric field, to model also the cathode fall of abnormal glow discharge [40, 46]. The failure of these attempts led to intense debate [39, 40, 44, 46, 48], recently clarified by Donkó and coworkers [39, 44]. Using a hybrid model, they showed that the different electric field distributions result in dissimilar energy distributions of species bombarding the cathode, thereby modifying the effective electron yield. This points to the important fact that the electron emission yields induced by ions and neutrals ($\gamma_{\mathrm{i}}(E)$ and $\gamma_{\mathrm{a}}(E)$) can be used in the simulations, but the effective yield γ' has to be calculated under the actual discharge conditions.

The analytical expressions for γ_{i} [30, 46] were recently used in modeling the breakdown behavior in radiofrequency argon discharges [49]. The dependence of γ_{i} on the incidence angle θ was included and taken to be $\propto 1/\cos\theta$.

It was found that, at low gas pressures, the breakdown voltage is a multivalued function of pressure, i.e., a single pressure corresponds to several breakdown voltages [50]. The multivalued branch of the breakdown curve could be reproduced only by taking into account the energy dependence of the ion-induced secondary electron emission yield. The inclusion of the angular dependence of the yield improved the agreement with experimental data.

It is important to remark that many of the above-mentioned studies used the yields γ_{i} and γ_{a} for "dirty" metal surfaces. However, it is known that, for untreated metal surfaces, the KEE yields decrease with successive sputtering cycles as contaminants are removed [47] while, at energies below a few hundred eV, the PEE yields increase upon sputter cleaning. Furthermore, changes in the electron emission yields, due to spatial and temporal modification of the surfaces of electrodes during the discharge, can produce plasma nonuniformities and instabilities in discharge parameters [51], which are major concerns in plasma-based processing of materials, such as film growth and etching.

We now consider the magnetically assisted magnetron glow discharges, where secondary electrons are trapped in the region near the cathode by an external magnetic field. The electron confinement allows operation at low pressures of a few millitorrs with typical applied voltages between 200 and 500 V, making the magnetron discharge very convenient for sputter deposition. The magnetic field strength is adjusted to avoid affecting the ions, which are extracted from the plasma and hit the cathode, where they give rise to sputtering and electron emission. Models of the magnetron discharge [35, 42], discussed in the following section of the book, show that sputtering is predominantly determined by ions of the buffer gas, with a much smaller contribution of fast neutral and a marginal contribution of sputtered target particles. Therefore, electron emission from the cathode is primarily determined by ion impact.

The dependence of the magnetron discharge characteristics on secondary electron yields has been investigated by self-consistent calculations. As an example, Kondo and Nanbu [52] found with a Monte Carlo model a substantial decrease in both the electron density and ionization rate when decreasing γ from 0.15 to 0.12. Shidoji et al. [53] discussed the influence of the electron yield on the current–voltage characteristic of the Ar discharge using a hybrid model, with $\gamma = 0.0005\,V_{\mathrm{a}}$, where V_{a} is the applied voltage (in the range 240–400 V). The authors found that the V_{a} in the simulated J–V characteristic was lower than the experimental value obtained with a Cu cathode, and an agreement required halving the value of γ, which they state would make it too small compared to experimental values. The authors attributed the discrepancy to diffusion loss of electrons.

2.4.1 Effect of Electron Recapture at the Cathode

Inelastic collisions and a fraction of elastic collisions prevent the ejected electrons from returning to the cathode. However, since the electron mean free

path is inversely proportional to pressure, at the low gas pressures of a magnetron discharge [42,54,55], a significant number of these electrons can return to the cathode and be recaptured without producing ionizations. The effect of electron recapture on the argon discharge characteristics has been discussed in a simplified [54] and a detailed model of the dc planar magnetron [42]. Since electron emission from the cathode is primarily determined by ion impact, the effective electron emission yield is given by [42]

$$\gamma' = \frac{N_{\mathrm{ej}} - N_{\mathrm{rec}}}{N_{\mathrm{ion}}} = \gamma'_{\mathrm{ion}} - \frac{N_{\mathrm{rec}}}{N_{\mathrm{ion}}}, \tag{2.7}$$

where N_{ej} is the rate of electrons produced by ion impact, N_{rec} the rate of electrons recaptured at the cathode, and N_{ion} the rate of ion impacts on the cathode. The effective electron yield without recapture, i.e., only due to ion impact at the cathode, is given by $\gamma'_{\mathrm{ion}} = N_{\mathrm{ej}}/N_{\mathrm{ion}}$. The authors calculated γ'_{ion} using the energy-dependent expression for γ_{i} given for clean metal surfaces [30]. For these types of surfaces, Fig. 2.1 shows that at the Ar^+ energies typical of a magnetron discharge electron emission is determined by PEE with a nearly constant yield. The effective yield γ' is a function of the pressure and the electron reflection coefficient RC, which in turn depends on the cathode material, including contaminant layers. Kolev and Bogaerts [42] calculated that γ' is significantly reduced by electron recapture and exactly one half of γ for the intermediate value of RC = 0.5.

The influence of different discharge parameters on the discharge voltage during magnetron sputtering has been recently discussed by Depla et al. [55] who compiled a list of electron emission yields for several metals from experimental data and empirical formulas found in literature [47,56,57]. As seen in Fig. 2.3, the discharge voltage for constant current operation of the magnetron resulted inversely proportional to the PEE yield of the target material [58]. This finding can be understood on the basis of the well-known equation proposed by Thornton [59] for V_{min}, the minimum discharge voltage to sustain a magnetron discharge,

$$V_{\mathrm{min}} = \frac{W_0}{\gamma' \varepsilon_{\mathrm{i}} \varepsilon_{\mathrm{e}}}, \tag{2.8}$$

where W_0 is the effective ionization energy ($\approx$30 eV for Ar^+), ε_{i} the ion collection efficiency, and ε_{e} the fraction of the maximum number of ions V_{min}/W_0 that can be made on average by a primary electron before it is lost from the system. Expressing the effective yield γ' as the product of the ion-induced electron emission yield of the target material γ_{i} and the effective gas ionization probability $E(p)$ [56], we get

$$V_{\mathrm{min}} = \frac{W_0}{E(p) \gamma_{\mathrm{i}} \varepsilon_{\mathrm{i}} \varepsilon_{\mathrm{e}}}. \tag{2.9}$$

Assuming a material-independent recapture probability and a constant pressure leads to the inverse proportionality between the discharge voltage and γ_{i}, reported in Fig. 2.3.

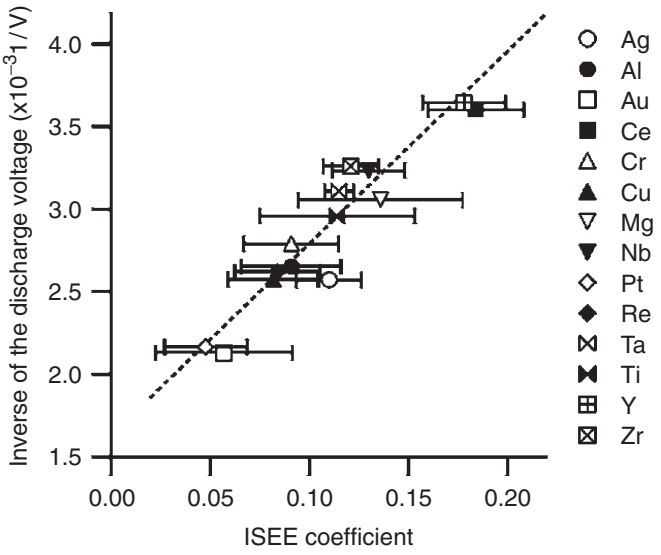

Fig. 2.3. The inverse of the measured discharge voltage V_{Ar} as a function of the electron emission yields shown in the *horizontal axis*, for different metallic targets, measured at a constant current of 0.3 A and argon pressure of 0.3 Pa. The error bars are based on the minimum and maximum values reported in the literature (from [55])

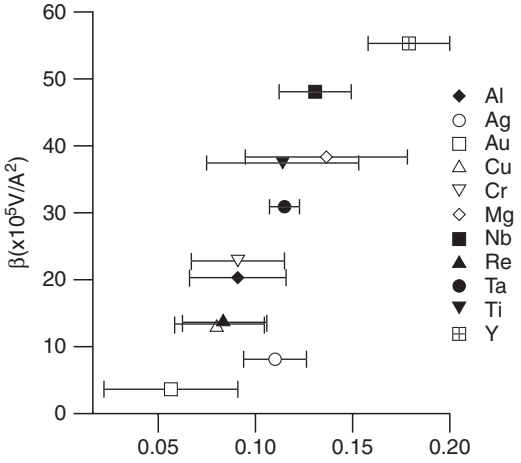

Fig. 2.4. The influence of the electron emission yields (*horizontal axis*) on the coefficient β (from [56])

The electron emission properties of the cathode material influence also the I–V characteristics of the discharge. The measured I–V curves [56] have been reproduced by the equation $I = \beta(V - V_{\mathrm{min}})^2$ [60], where β is a constant. As shown in Fig. 2.4, the value of β increases with increasing γ_{i}. As discussed

in [56] this is because, for a fixed discharge voltage, a higher γ_i produces a higher plasma density [52], which means a lower plasma impedance and, therefore, a higher value of β.

2.4.2 Effect of Changes in the Chemical Composition of the Cathode

It is noteworthy that, for some target materials (Al, Cr, Mg, Nb, Re, Ti) at low discharge current, the discharge voltage decreases with increasing current [55], possibly due to target contamination by residual gases during sputtering. Indeed, since water is the main species in the residual gas, its chemisorption on target surfaces cannot be ruled out, especially at low discharge current. Chemisorption is critical in reactive magnetron sputtering of a metallic target, where a reactive gas is added to the discharge to deposit a compound material. The addition of the reactive gas results in the formation of a compound material not only on the substrate (anode) but also on the target (cathode) where its formation is balanced by the sputtering process. This changes the electron emission properties of the cathode which, together with the modification of the plasma composition, changes the plasma impedance. At a constant discharge current, this change of the plasma impedance results in a change of the discharge voltage. Whether the voltage increases or decreases with respect to the discharge voltage with metallic targets depends on the target material [61–63]. It has been found [60] that the discharge voltage during reactive sputtering of aluminum decreases when adding oxygen or nitrogen, in contrast to the case of other metallic targets. The difficulty in the understanding of these contrasting behaviors is that both the target condition and the plasma composition change when adding the reactive gas.

A series of interesting experiments [58, 64] have been recently performed to study the behavior of the discharge voltage, at constant current, during reactive sputtering of oxides. In these experiments, the metal target is first sputtered in pure Ar until a constant discharge voltage, V_{Ar}, is established. Then Ar was replaced by pure oxygen and the new discharge voltage, $V_{\mathrm{O_2}}$, was measured. In a third step, O_2 was replaced with Ar and the discharge voltage with the oxidized target, $V_{\mathrm{ox,Ar}}$, was measured. In this way $V_{\mathrm{ox,Ar}}$ can be directly compared to V_{Ar}, since both are measured under identical experimental conditions and plasma composition. As shown in Fig. 2.3, the measured discharge voltage for metallic targets V_{Ar} is inversely proportional to the ion-induced electron emission yield γ_i of the target. A straight line can be fitted to the data in Fig. 2.3

$$\frac{1}{V_{\mathrm{Ar}}} = A + B\gamma_i. \tag{2.10}$$

Given the fitting coefficient A and B, which are only valid for a given series of experiments because they depend on the experimental conditions (discharge

current, pressure, and magnetic field), the authors attempted to extract the electron emission yield of the oxidized target as

$$\gamma_{\mathrm{i,ox}} = \frac{1}{B}\left(\frac{1}{V_{\mathrm{ox,Ar}}} - A\right). \tag{2.11}$$

The literature data for ion-induced emission yield of oxides are scarce. For magnesium oxide, the authors found a value of 0.4, which is of the same order magnitude of the value of 0.2, measured by ion beam experiments [65,66]. We note here that the yield obtained by this procedure should be more properly compared with the effective yield without recapture, γ'_{ion} as defined in (2.7), and may not be directly compared with ion beam-induced emission yields γ_{i}. In fact, (2.9) and (2.10) are based on a compilation of PEE yields for clean metal surfaces, i.e., constant yield γ_{i} in the ion energy range of interest for magnetron discharge for which $\gamma'_{\mathrm{ion}} = \gamma_{\mathrm{i}}$ (see, e.g., (2.6)). For dirty or oxidized surfaces and in general for KEE, there will be differences between γ_{i} and γ'_{ion}, this last being determined by the dependence of γ_{i} on ion energy and by the ion energy distribution at the applied discharge voltage. The extent of this difference will depend on the narrowness of the ion energy distribution, but it should be carefully taken into account as it can be a source of discrepancy when comparing electron emission yields obtained by different experimental techniques and procedures.

Another source of discrepancy may be the assumption of a constant probability of recapture of electrons at the cathode. Chemisorption affects the electron recapture at the cathode and hence the effective ionization probability. As shown by Babout et al. [67] for copper, the electron reflection coefficient decreases with oxygen exposure, i.e., recapture becomes more important.

A remarkable finding of these experiments is that two groups of materials could be distinguished from the analysis discussed above: one where the electron yield increases on oxidation (Al, Ce, Li, Mg, Y) and one where it decreases (Cr, Nb, Re, Ta, Ti). This finding is in apparent contrast with the generally accepted idea that oxide materials have larger yields than metals, although it is not inconsistent with the different behavior of Al and Mo upon oxidation [27], mentioned above. A suggestion for the uneven behavior of different materials upon oxidation has been proposed based on a study by Wittmaack [68] of electron emission from n-type silicon bombarded with O^+ and O_2^+ ions. A conclusion of this work is that the enhanced electron yield generated by oxygen implantation in silicon is directly proportional to the fractional coverage of the surface with SiO_2 islands growing at the bombarded surface. Isolated oxygen atoms embedded in Si or suboxides (SiO_x, $x < 2$) apparently produce only a negligible change in the electron yield. This interpretation, however, has not been accompanied by arguments based on electron excitation, transport, and escape mechanisms. Based on Wittmaack's work, Depla et al. [58] concluded that the discharge voltage behavior during reactive sputtering of metal oxides originates in the formation of an oxide layer of the order of 1–2 nm, as estimated from the sum of the ion range and the straggle

of the oxygen implanted during the plasma oxidation. The formation of this oxide layer changes the electron yield of the target; depending on the type of oxide formed during plasma oxidation and subsequent sputtering in argon, the yield is high (oxides) or low (suboxides). The low yield of suboxides is a very interesting feature that has not yet been elucidated and deserves further investigations with the use of in situ surface analysis techniques.

2.5 Outlook

The description of the understanding of physical mechanism and its application to some types of gaseous discharges points to directions for research. The most important variable in electron emission seems to be the state of the surface, which changes dynamically during the operation of the electric discharge. This is because of the competition of sputtering which removes native surface contamination and chemical alterations due to ion implantation (in reactive discharges) and recondensation of impurities from surfaces in the vacuum system. Possibly the most promising first step would be the study of electron emission yields using reactive gas ions over a range of targets, incident energies, and accumulated ion fluences. Fundamental studies need to relate observed changes in electron yields to measured changes in surface composition, as determined, e.g., by X-ray photoelectron spectroscopy. This is particularly important to understand the materials dependence of the changes of electron yield upon oxidation.

References

1. J. Schou, in *Physical Processes of the Interaction of Fusion Plasmas with Solids*, Chap. 5, ed. by W.O. Hofer and J. Roth (Academic, New York, 1996)
2. K. Töglhofer, F. Aumayr, H.P. Winter, Surf. Sci. **281**, 1430 (1993)
3. D. Hasselkamp, H. Rothard, K.-O. Groeneveld, J. Kemmler, P. Varga, H. Winter, *Particle Induced Electron Emission II* (Springer, Berlin Heidelberg New York, 1992)
4. R.A. Baragiola (ed.), *Ionization of Solids by Heavy Particles* (Plenum, New York, 1993)
5. R.A. Baragiola, in *Low Energy Ion-Surface Interactions*, Chap. 4, ed. by J.W. Rabalais (Wiley, New York, 1994)
6. H. Kudo, *Ion-Induced Electron Emission from Crystalline Solids* (Springer, Berlin Heidelberg New York, 2001)
7. H. Winter, H. Burgdörfer (eds.), *Slow Heavy-Particle Induced Electron Emission from Solid Surfaces* (Springer, Berlin Heidelberg New York, 2007)
8. B.A. Brusilovsky, Appl. Phys. A **50**, 111 (1990)
9. S. Valeri, Surf. Sci. Rep. **17**, 85 (1993)
10. R.A. Baragiola, Radiat. Eff. **61**, 47 (1982)
11. H.D. Hagstrum, in *Chemistry and Physics of Solid Surfaces VII*, ed. by R. Vanselow, R.F. Howe (Springer, Berlin Heidelberg New York, 1988), p. 341

12. R.A. Baragiola, E.V. Alonso, A. Oliva, Phys. Rev. B **19**, 121 (1979)
13. H. Winter, S. Lederer, H.P. Winter, Europhys. Lett. **75** (6), 964 (2006)
14. G.E. Zampieri, F. Meier, R.A. Baragiola, Phys. Rev. A **29**, 116 (1984)
15. J.W. Rabalais, H. Bu, C.D. Roux, Phys. Rev. Lett. **69**, 1391 (1992)
16. H. Winter, F. Aumayr, G. Lakits, Nucl. Instrum. Meth. Phys. Res. B **58**, 301 (1991)
17. R.A. Baragiola, Nucl. Instrum. Meth. B **78**, 223 (1993)
18. R.C. Amme, J. Chem. Phys. **50**, 1891 (1969)
19. B.L. Schram, A.J.H. Boerboom, W. Kleine, J. Kistemaker, Physica **32**, 749 (1966)
20. L.A. Dietz, J.C. Sheffield, J. Appl. Phys. **46**, 4361 (1975)
21. E.V. Alonso, M. Alurralde, and R.A. Baragiola, Surf. Sci. **166**, L155 (1986)
22. G. Lakits, F. Aumayr, M. Heim, H. Winter, Phys. Rev. A **42**, 5780 (1990)
23. P.M. Waters, Phys. Rev. **111**, 1053 (1958)
24. H.S.W. Massey, E.H.S. Burhop, and H.B. Gilbody, *Electronic and Ionic Impact Phenomena*, Chap. 17 (Clarendon, Oxford, 1971)
25. Y.N. Demkov, I.V. Komarov, Sov. Phys. JETP **23**, 1989 (1966)
26. M.E. Rudd, Phys. Rev. A **38**, 6129 (1988)
27. J. Ferrón, E.V. Alonso, R.A. Baragiola, A. Oliva-Florio, Surf. Sci. **120**, 427 (1982)
28. N. Bajales, S. Montoro, E.C. Goldberg, R.A. Baragiola, J. Ferrón, Surf. Sci. Lett. **579**(2–3), 97 (2005)
29. M. Negre, J. Mischler, and N. Bénazeth, Surf. Sci. **157**, 436 (1985)
30. A.V. Phelps and Z. Lj. Petrovic, Plasma Sources Sci. Technol. **8**, R21 (1999)
31. E.V. Alonso, R.A. Baragiola, J. Ferrón, A. Oliva-Florio, Radiat. Eff. **45**, 119 (1979)
32. A. Bogaerts, J. Anal. Atom. Spectrom. **22**, 13 (2007)
33. A. Bogaerts, K. De Bleecker, I. Kolev, M. Madani, Surf. Coat. Technol. **200**, 62 (2005)
34. A. Bogaerts, K. De Bleecker, V. Georgieva, I. Kolev, M. Madani, E. Neyts, Plasma Process. Polym. **3**, 110 (2006)
35. I. Kolev, A. Bogaerts, Plasma Process. Polym. **3**, 127 (2006)
36. M. Surendra, D.B. Graves, G.M. Jellum, Phys. Rev. A **41**, 1112 (1990)
37. A. Bogaerts, R. Gijbels, Phys. Rev. A **52**, 3743 (1995)
38. R.E. Robson, R.D. White, Z. Lj. Petrovic, Rev. Mod. Phys. **77**, 1303 (2005)
39. Z. Donkó, P. Hartmann, K. Kutasi, Plasma Sources Sci. Technol. **15**, 178 (2006)
40. A.V. Phelps, Plasma Sources Sci. Technol. **10**, 329 (2001)
41. A. Bogaerts, R. Gijbels, Plasma Sources Sci. Technol. **11**, 27 (2002)
42. I. Kolev, A. Bogaerts, R. Gijbels, Phys. Rev. E **72**, 056402 (2005)
43. P. Hartmann, Z. Donkó, G. Banó, L. Szalai, K. Rósza, Plasma Sources Sci. Technol. **9**, 183 (2000)
44. Z. Donkó, Phys. Rev. E **64**, 026401 (2001)
45. M. Radmilović-Radjenović, J.K. Lee, Phys. Plasmas **12**, 063501 (2006)
46. A.V. Phelps, L.C. Pitchford, C. Pedoussat, Z. Donkó, Plasma Sources Sci. Technol. **8**, B1 (1999)
47. R.A. Baragiola, E.V. Alonso, J. Ferron, A. Oliva-Florio, Surf. Sci. **90**, 240 (1979)
48. A.P. Bokhan, P.A. Bokhan, D.E. Zakrevsky, Appl. Phys. Lett. **86**, 151503 (2005)
49. M. Radmilović-Radjenović, J.K. Lee, Phys. Plasmas **12**, 063501 (2006)
50. V.A. Lisovskiy, V.D. Yegorenkov, J. Phys. D: Appl. Phys. **32**, 3349 (1998)

51. E.V. Barnat, G.A. Hebner, J. Appl. Phys. **98**, 013305 (2005)
52. S. Kondo, K. Nanbu, J. Phys. D: Appl. Phys. **32**, 1142 (1999)
53. E. Shidoji, K. Ness, T. Makabe, Vacuum **60**, 299 (2001)
54. G. Buyle, W. De Bosscher, D. Depla, K. Eufinger, J. Haemers, R. De Gryse, Vacuum **70**, 29 (2003)
55. G. Buyle, D. Depla, K. Eufinger, R. De Gryse, J. Phys. D: Appl. Phys. **37**, 1639 (2004)
56. D. Depla, G. Buyle, J. Haemers, R. De Gryse, Surf. Coat. Technol. **200**, 4329 (2006)
57. L.M. Kishnevskiy, Radiat. Eff. **19**, 23 (1973)
58. D. Depla, S. Heirweigh, S. Mahieu, J. Haemers, R. De Gryse, J. Appl. Phys. **101**, 013301 (2007)
59. J.A. Thornton, J. Vac. Sci. Technol. **15**(2), 171 (1978)
60. W.D. Westwood, S. Maniv, P.J. Scanlon, J. Appl. Phys. **54**, 6841 (1983)
61. R. Mientus, K. Ellmer, Surf. Coat. Technol. **116–119**, 1093 (1999)
62. D. Depla, R. De Gryse, Plasma Sources Sci. Technol. **10**, 547 (2001)
63. D. Depla, J. Haemers, R. De Gryse, Plasma Sources Sci. Technol. **11**, 91 (2002)
64. D. Depla, J. Haemers, R. De Gryse, Thin Solid Films **515**, 468 (2006)
65. P. Riccardi, M. Ishimoto, P. Barone, R.A. Baragiola, Surf. Sci. **571**, L305 (2004)
66. W.S. Vogan, R.L. Champion, V.A. Esaulov, Surf. Sci. **538**, 211 (2003)
67. M. Babout et al., J. Phys. D: Appl. Phys. **10**, 2331 (1977)
68. K. Wittmaack, Surf. Sci. **419**, 249 (1999)

http://www.springer.com/978-3-540-76664-3

Reactive Sputter Deposition
Depla, D.; Mahieu, S. (Eds.)
2008, XVIII, 572 p.,
ISBN: 978-3-540-76664-3